

# Computational organic chemistry

Kelvin Jackson, Sami K. Jaffar and Robert S. Paton\*

DOI: 10.1039/c3oc90007j

This review summarizes advances made in the field of computational organic chemistry in 2012, focussing on the following topics: (1) organic structure and bonding, (2) organo-catalytic mechanisms, (3) computational structural elucidation, (4) dynamic effects, (5) methodological advances and (6) computational organic chemistry on the web.

## 1 Introduction

The purpose of this report is to gather together literature from 2012 that may reasonably be termed *computational organic chemistry*. We have interpreted this term in a broad sense, bringing together highlights of recent achievements in the computational study of organic structure and bonding, reaction mechanism and selectivity, reaction dynamics and structural prediction, along with some recent developments in methodologies for computational organic chemistry. We feel this gives a broad overview of some key research themes in the field. Inevitably, there are far more good papers published in a single year than may be reasonably covered in such a review, and so our intention has been to define the state of the art with some of the illustrative examples from 2012. We aim to whet the appetite of scholar and student alike, continuing the good work of Prof. Steven Bachrach, who has ably written this annual report during the years 2008–2012.<sup>1–5</sup>

## 2 Organic structure and bonding

In organic chemistry qualitative or semi-quantitative terms such as strain or aromaticity abound, being used routinely to rationalize experimental results and computational predictions. Computation offers various means to probe the underlying assumptions behind such statements and on occasion to quantify such effects, as illustrated in this section.

### 2.1 Hyperconjugation and conjugation

In 2012 Corminboeuf and co-workers published a helpful tutorial review<sup>6</sup> on the subject of computing what they term “fuzzy” chemical concepts: contemporary

---

Chemistry Research Laboratory, University of Oxford, 12 Mansfield Road, Oxford OX1 3TA, UK.  
E-mail: robert.paton@chem.ox.ac.uk

methods for quantifying the chemical bond, atomic charges, conjugation and hyperconjugation and strain energies are all explored. As is pointed out, different interpretations may result from the application of contrasting computational methods. For example, the importance of some stereoelectronic interactions in the anomeric effect has recently been challenged in computational studies by Mo.<sup>7</sup> Using the Block-localized wavefunction (BLW) method,<sup>8</sup> which constructs and optimizes a full set of orthogonal molecular orbitals for a single Valence Bond (VB) structure, Wu and Mo<sup>9</sup> have analysed stereoelectronic effects in relation to the anomeric effect. For 2-methoxyoxane the BLW computed delocalization energy is greater in the  $\alpha$ -anomer by 6.6 kJ mol<sup>-1</sup>, while exchange repulsion favours the  $\beta$ -anomer by 10.4 kJ mol<sup>-1</sup>, which coupled with dispersion effects leads to the observed anomeric preference for the  $\beta$ -anomer. The BLW approach leads to smaller estimates for hyperconjugative interactions relative to a Natural Bond Orbital (NBO) analysis, as has been shown previously in the case of ethane.<sup>10</sup> NBO calculations transform the set of occupied canonical MOs obtained from an electronic structure calculation into the set of NBOs without altering the overall electron distribution or total energy. Delocalization between occupied and unoccupied orbitals is then quantified using the off-diagonal elements in the Fock matrix. In contrast the BLW approach is to begin from a single localized VB (*i.e.* resonance) structure followed by a self-consistent optimization of the MOs. This then leads to a lower energy gap between the delocalized reference and the electron-localized BLW structure than would be the case for the corresponding localized NBO structure, and so the BLW delocalization energies are smaller in magnitude.

Schleyer has explored the role of hyperconjugative interactions in the conformational preference of cyclooctatetraene (COT).<sup>11</sup> While the nonplanar minimum is typically ascribed to the avoidance of a Huckel anti-aromaticity, it is shown that delocalization from CC/CH  $\sigma$  to CC  $\pi^*$  and also from CC  $\pi$  to CC/CH  $\sigma^*$  orbitals leads to the preferential adoption of the tub-shaped  $D_{2d}$  form of COT. This is termed “two-way” or double hyperconjugation, shown in Fig. 1. Homodesmotic reaction energies<sup>12</sup> support the idea that tub-shaped COT benefits from thermodynamically stabilizing interactions. The near-parallel alignment of the CC  $\sigma$ , CH  $\sigma$  and CC  $\pi$  orbitals as shown above, makes “two-way” hyperconjugation possible. BLW calculations (HF/6-31G(d)) support the viewpoint that the ground state (GS)  $D_{2d}$  and transition structure (TS)  $D_{2h}$  of COT are equally delocalized, the former through hyperconjugation, the latter through  $\pi$ -conjugation, so that the barrier for flipping results principally from steric contributions. This is further supported by NBO analysis (B3LYP/6-311+G(d,p)). Borden has reported calculations at the B3LYP/6-31G(d) level on

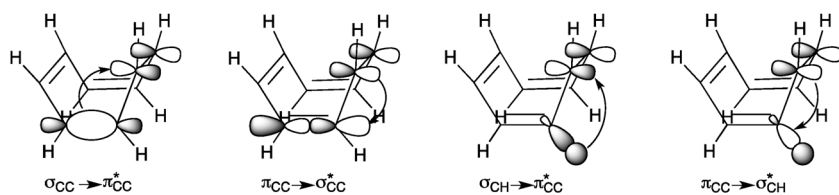


Fig. 1 Hyperconjugation in the tub form of cyclooctatetraene (COT).

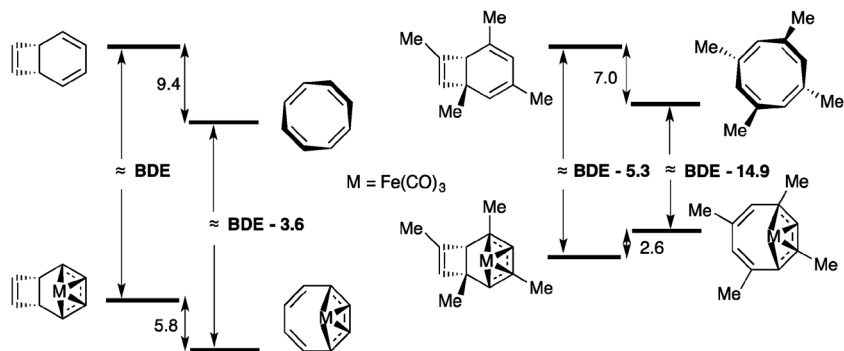


Fig. 2 Binding ( $\text{kcal mol}^{-1}$ ) of COT and TMCOT to  $\text{Fe}(\text{CO})_3$ .

the relative energetics of COT and its isomer bicyclo[4.2.0]octa-2,4,7-triene (BCOT) that results from electrocyclic ring closure, and on the relative of both structures with  $\text{Fe}(\text{CO})_3$ .<sup>13</sup> While COT is more stable than BCOT by some  $9.4 \text{ kcal mol}^{-1}$ , the complexes with  $\text{Fe}(\text{CO})_3$  only differ by  $5.8 \text{ kcal mol}^{-1}$ . Decomposition of the binding energies into deformation and interaction terms show that the interaction for COT is more favourable by  $9.8 \text{ kcal mol}^{-1}$ , however, the distortion required for partial planarization from the  $D_{2d}$  tub form is more difficult than for BCOT (Fig. 2). For 1,3,5,7-tetramethylcyclooctatriene (TMCOT) and its isomer TMBCOT, the preferred complex is now formed with TMBCOT. The preferential stability of TMCOT is reduced by  $2.4 \text{ kcal mol}^{-1}$  relative to the unsubstituted case, however, there is a much more significant change in the relative binding energies of the two forms, with TMCOT complexation to  $\text{Fe}(\text{CO})_3$  now less favourable than that of TMBCOT by  $6.0 \text{ kcal mol}^{-1}$ . This is attributed in large part ( $3.6 \text{ kcal mol}^{-1}$ ) to the unfavourable allylic strain developed upon partial planarization of TMCOT in the complex, which is more severe for methyl-substituted double bonds.

Wu and Schleyer discuss the factors contributing to the instability of cyclobutadiene (CBD).<sup>14</sup> While this molecule is often held up as the archetypal example of antiaromaticity, the authors remark “*instead of the conventional interpretation of CBD as the antiaromatic paradigm, it should be regarded as a unique molecule*”. This statement is prompted by an analysis of the isodesmic reaction energy relating CBD with *s-trans* butadiene and ethylene, shown below. The reaction is unfavourable by  $81.5 \text{ kcal mol}^{-1}$  (B3LYP/PVTZ), however, using BLW calculations with  $\pi$ -conjugation “turned off”, the reaction energy is still unfavourable by  $62.2 \text{ kcal mol}^{-1}$ . Thus it would appear that the ring strain of CBD, which includes angular strain,  $\pi$ - $\pi$  repulsion, and torsional strain is the most significant factor in the destabilization of CBD. Antiaromatic destabilization is predicted to contribute only 20% of the overall ( $77.2 \text{ kcal mol}^{-1}$ ) destabilization as shown in Fig. 3.

Schleyer has also investigated the conformational preferences of four-membered rings containing two  $\pi$ -electrons, such as the cyclobutadienyl dication,  $\text{C}_4\text{H}_4^{2+}$ .<sup>15</sup>

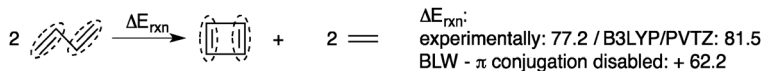


Fig. 3 Estimating the destabilization of cyclobutadiene.

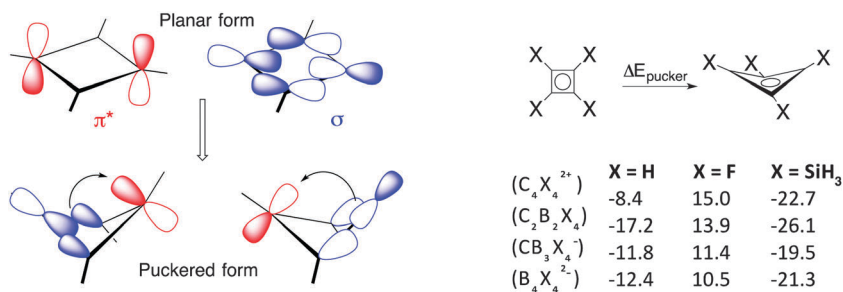


Fig. 4 Hyperconjugation stabilizes ring-puckering of 2-electron rings.

The observed non-planarity of such systems is perhaps surprising on the basis of expected Huckel aromaticity, and so explanations based either on p-orbital 1,3-bonding interactions or on hyperconjugative  $\sigma$ - $\pi^*$  interactions have been advanced. Calculations (B3LYP/6-311+G(d,p)) support the idea that hyperconjugative interactions are indeed the cause behind the non-planarity, in which distortion from  $D_{4h}$  to lower symmetry enables mixing between donor  $\sigma$ -orbitals and ring p-orbitals. (Fig. 4) The molecule  $B_4H_4$ , for which there are no p-electrons to favour 1,3-interactions, also adopts a puckered conformation and B-B  $\sigma$ -bonding MOs are computed to become stabilized upon puckering. Silyl substituents on the cyclobutadienyl dication also lead to a greater preference for puckered forms through greater hyperconjugative delocalization, while fluorine substitution reduces this effect and in fact leads to a preference for the planar form.

## 2.2 Stereoelectronic effects and aromaticity in transition structures

Computational studies may be used to gain insight into transition structures in a way that may not be possible experimentally. Energy decomposition schemes such as those already discussed above are not limited to the study of ground state structures, and have also been used to understand structure and bonding in transition structures of organic reactions. Alabugin and co-workers have investigated the copper-free “click” reaction of an alkyne and azide, a cycloaddition which often uses highly reactive, strained, alkynes to achieve acceptable reaction rates.<sup>16</sup> In pursuing a strategy to stabilize the TS for this reaction rather than destabilize the ground state, stabilization of the alkyne HOMO was targeted. The activation barriers of nucleophilic additions and cycloadditions involving alkynes show a correlation with the deformation energy of the CC triple bond,<sup>17</sup> and so a suitably oriented electron acceptor group is able to facilitate alkyne bending through hyperconjugative CC  $\pi$ -CX  $\sigma^*$  delocalization. As shown in Fig. 5a the alkyne ground state structure is able to bend more easily due to the greater delocalization of the CC- $\pi$  into acceptor CX  $\sigma^*$  orbital, which, viewed through the lens of the distortion-interaction model of reactivity leads to a smaller distortion energy term and hence greater reactivity. In the cycloaddition TS itself, negative hyperconjugation between the CX  $\sigma^*$  orbital and the  $\pi^*$  + HOMO<sub>azide</sub> contributes an additional stabilizing stereoelectronic interaction that further decreases the barrier height.

Alabugin has also studied the 5-*endo*-dig cyclization of alkynes.<sup>18</sup> M05-2X activation energies showed this reaction to be anomalously fast in relation to the 4-*endo*-dig and 6-*endo*-dig analogues, proceeding *via* a much earlier TS with a

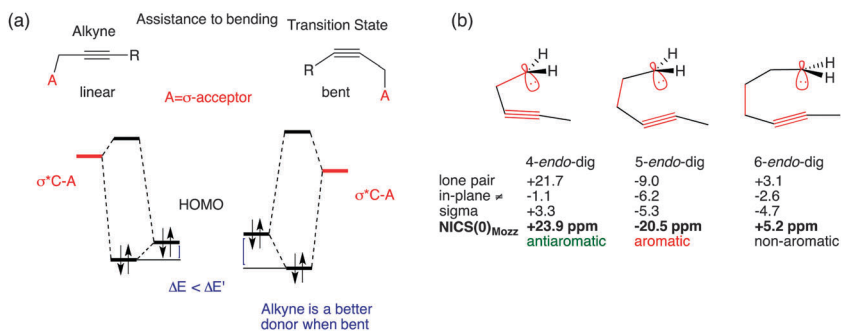


**Fig. 5** (a) Hyperconjugation due to alkyne bending in cycloadditions; (b) classification of TS aromaticity with NICS calculations.

longer forming bond. Calculation of nuclear independent chemical shifts (NICS) values at the ring centre was performed to evaluate the aromaticity in the TS.<sup>19</sup> Care was taken to use the NICS(0)<sub>MOzz</sub> values, obtained from a natural chemical shielding analysis, which uses only the component of the shielding tensor perpendicular to the ring due to the MOs contributing to “in-plane aromaticity” (Fig. 5b). These computed NICS(0)<sub>MOzz</sub> values show that the 4-endo TS is antiaromatic, the 6-endo TS is non-aromatic, whilst the 5-endo-dig TS is aromatic, with an appreciably negative NICS value. Since this constitutes an aromatic TS for a non-pericyclic reaction, the authors argue the reaction is in fact an “aborted” [2,3]-sigmatropic shift, in which the reaction is stopped at the cyclized form since it lies much lower in energy than the product that would be obtained from the [2,3]-rearrangement.

### 2.3 Valence bond structures and bonding in C<sub>2</sub>

Shaik, Rzepa and co-workers have recently analyzed the bond in the C<sub>2</sub> diatomic using valence bond (VB) theory and the full configuration interaction (CI) approach (Fig. 6).<sup>20</sup> The MO diagram is suggestive of only a double bond, while using sp hybridized carbons the picture is of a triple bond, with two sp hybrids pointing outwards. The ground state of C<sub>2</sub> is a singlet, so these electrons are spin-coupled: here it is argued that this in fact constitutes a fourth bond in C<sub>2</sub>, the energy of which may be quantified. The VB/6-31G(d) approach is used to evaluate the *in situ* bond energy ( $D_{in}$  in Fig. 6), defined with regard to a pair of electrons relative to the two separated carbon atoms in their “prepared” <sup>5</sup>S state without electronic relaxation from the molecule, to give a value of 14.3 kcal mol<sup>-1</sup>. In the CI approach, this bond energy may be defined as approximately half the energy for the singlet–triplet gap (neglecting overlap the triplet state is repulsive by the same amount as the singlet state is bonding, and this is the electron pair spin exchange term), 14.8 kcal mol<sup>-1</sup>, compared with an experimental value of 13.2 kcal mol<sup>-1</sup>. Both theoretical approaches emphasize the population of the bonding 3 $\sigma_g$  MO in contributing the fourth bond: in the VB picture the fourth bond is formed as a weighted sum of 2 $\sigma_u^*$  and 3 $\sigma_g$  orbitals, while the second most important configuration in the CI picture, which has a coefficient of 0.32, has this 3 $\sigma_g$  bonding MO doubly occupied.

In 2012 the merits of approaches utilizing hybridized atomic orbitals (HAOs) in conceptualizing bonding has been discussed in a series of articles in the

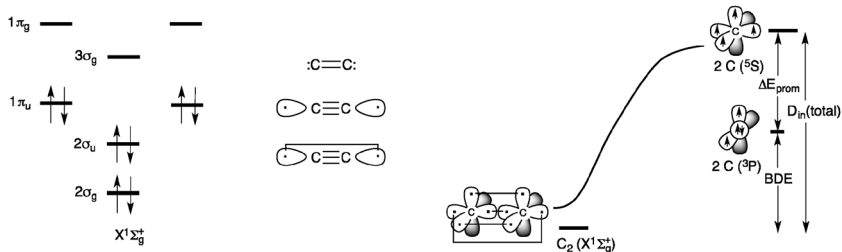


**Fig. 6** Pictures of bonding in  $C_2$  from left to right: the MO diagram, cartoon representations of doubly-bonded  $C_2$  with sp-lone pairs, singlet paired biradical or with a quadruple bond, and the definition of *in situ* bond energy in ref. 20.

*Journal of Chemical Education*. In response to an appeal in 2011<sup>21</sup> that, at least at the pedagogical level, the use of HAOs be discontinued, Landis<sup>22</sup> and Hiberty and Shaik<sup>23</sup> clearly set out the theoretical justification behind the use of HAO or other localized orbitals. Since transforming the canonical delocalized MOs, which are most commonly presented by electronic structure programs as the solutions to the SCF equations, into a set of localized MOs does not change the overall electron density or energy, both descriptions are correct. The question then is one of usefulness, and localized bonding models based on HAOs clearly find much use in organic chemistry, such as in rationalizing differences in acidities and bond lengths of alkanes, alkenes and alkynes. Reassuringly for organic chemists, when discussing basic valence shell electron pair repulsion (VSEPR) models, Hiberty and Shaik consider the nature of what “domains” best describe the location of electrons thus: “*What kind of orbitals describe these domains? As organic chemists know very well, these electron domains are just doubly occupied LMOs made of HAOs, which constitute the link between the Lewis structure and its quantum mechanical translation.*”

### 3 Organocatalytic reaction mechanisms

Organocatalysis, where small organic molecules are used to accelerate reactions and often to impart asymmetric induction, is an ever expanding area for organic synthesis, and computation has been essential in understanding aspects of mechanism and selectivity. Simón and Goodman have investigated a number of transformations catalyzed by chiral phosphoric acids in recent years,<sup>24</sup> establishing the dual role of the catalyst in activating both reacting partners, and also serving to rigidify the diastereomeric transition states, leading to high levels of stereoselection. In 2012, Goodman investigated the phosphoric acid catalyzed allylboration reaction, where the dual role of the catalyst was predicted from computation performed on a truncated model system (at the M06-2X/6-31G(d,p) level).<sup>25</sup> The acid enhances the Lewis acidity of boron by forming a hydrogen bond to the pinacol group attached to boron, while at the same time forming a contact to the aldehyde formyl proton with the other oxygen atom (Fig. 7). Mixed quantum mechanics/molecular mechanics (QM:MM) calculations were then employed combining B3LYP/6-31G(d) with UFF to investigate the full TS, giving good agreement in terms of the sense and level of asymmetric induction.

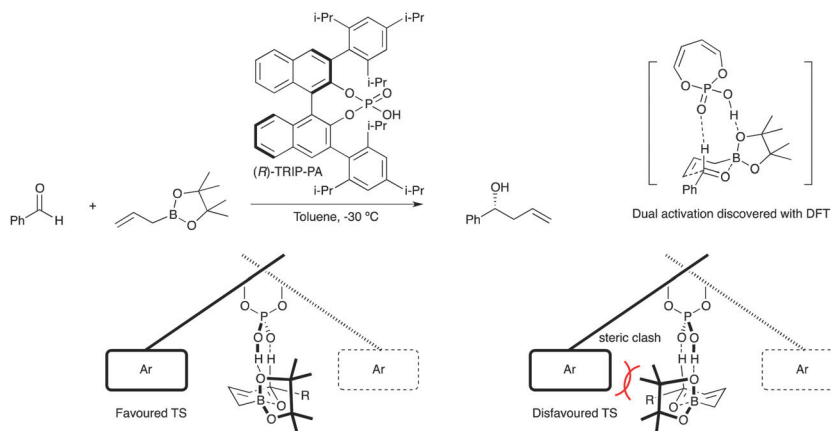


**Fig. 7** DFT derived model for catalysis in allylboration with chiral phosphoric acids, and model for asymmetric induction.

The enantioselectivity arises due to a clash between the pinacol group and the  $C_2$ -symmetric catalyst in the disfavoured transition structure. Simón and Goodman also investigated catalysis by an axially chiral guanidine in the reaction of  $\beta$ -ketoesters with azadicarboxylates.<sup>26</sup> Again QM:MM calculations (B3LYP:UFF) were used to explore the origins of the contrasting facial selectivity shown by cyclic and acyclic  $\beta$ -ketoesters, finding that an (*E*)-enolate geometry is adopted by the acyclic substrate, whereas the cyclic substrate must adopt a (*Z*)-enolate geometry.

The proline-catalyzed aldol reaction demonstrates the potential for use of naturally occurring amino acids as asymmetric catalysts and has inspired many organocatalytic variants. Houk has previously shown that DFT calculations may be used to understand the mechanism and stereocontrol in proline catalysis,<sup>27</sup> and even in the computer-aided design of modified amino acids.<sup>28</sup> Now Houk and Mahrwald have studied the role of histidine in catalyzed aldol additions, where both the role of the hydrogen bond donor and the origins of asymmetric induction are addressed at the M06-2X/6-31+G(d) level.<sup>29</sup> Competing transition structures for the reaction of isobutyraldehyde (shown as enamine) and chloroacetaldehyde are shown in Fig. 8, from which it can be seen that the preferred mode of activation is one *via* a hydrogen bond from the protonated imidazole group in the zwitterionic form of the amino acid. The computed selectivity from these TSs is in good agreement with the experimental levels of enantioselectivity, however, the stereochemical model to account for this selectivity contrasts with that applicable for previously studied proline-catalyzed reactions. Here, regardless of whether the imidazolium or carboxylic acid is acting as proton donor, the preferred orientation of the aldehyde puts the larger group in a pseudoaxial environment. The authors argue that for the disubstituted enamine formed from isobutyraldehyde studied, there is only one gauche interaction in the favoured TS while the disfavoured route has two such interactions.

Computation has also been used to probe the identity of intermediates in the catalytic cycle for the addition of aldehydes to nitroalkenes using a proline-derived organocatalyst.<sup>30</sup> Interestingly,  $\omega$ B97XD/6-311G(d,p) calculations found

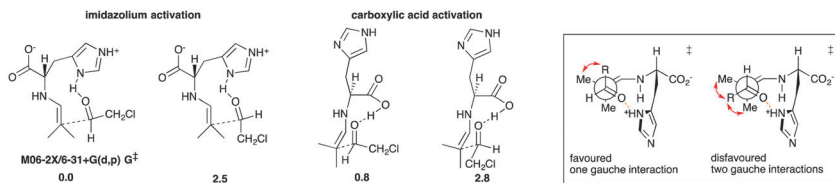


**Fig. 8** Comparison of different modes of Brønsted acid catalysis in the aldol reaction catalyzed by histidine and a model for enantioselectivity.

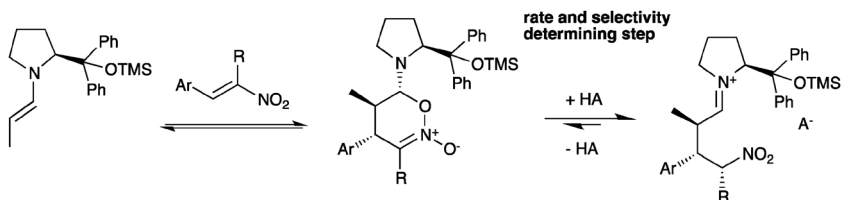


**Fig. 9** Discovery of a cyclic six-membered intermediate from DFT and experiment in organocatalytic conjugate additions.

that the product from the conjugate addition of an enamine derived from a diphenylprolinol silyl ether to an  $\alpha$ -substituted nitroalkene formed a cyclic 6-membered ring intermediate (corresponding to the formal [4+2] adduct) rather than the expected zwitterionic iminium nitronate species (Fig. 9). This intermediate is able to interconvert with a cyclobutane species that has previously been identified experimentally in the catalytic cycle. Calculation of the TSs for protonation of the cyclic intermediate shows relatively high barriers of 23.9 and 29.6 kcal mol<sup>-1</sup>, for the *Si* and *Re* modes, respectively, which suggest that this step governs the observed stereoselectivity and not C–C bond formation as previously thought. In support of this new hypothesis, the lower reactivity of  $\alpha$ -substituted nitroalkenes was also explained, in terms of the recalcitrance towards protonation of the cyclic intermediate formed; altering the  $\alpha$ -substituent from H to methyl stabilizes the relevant 6-membered ring intermediate by a further 4.4 kcal mol<sup>-1</sup>, resulting in a higher barrier for protonation.

## 4 Structural assignments

In recent years the use of quantum mechanical (QM) calculations for the prediction of measurable spectroscopic quantities such as NMR chemical shifts and coupling constants has seen a steady increase. As reviewed by Tantillo in 2012, the calculation of proton <sup>1</sup>H and carbon <sup>13</sup>C chemical shifts has become a useful tool for organic chemists to probe the structures of unknown natural (or synthetic) products by comparing the predicted spectra of candidate structures against an experimental spectrum.<sup>31</sup> Modern electronic structure packages now enable DFT computations of shielding tensors (and hence chemical shifts) to be performed with relative ease. However, a decision must also be made over which is the appropriate functional and basis set to use, and what is the appropriate internal standard, or whether to use empirically derived scaling parameters.

Helpfully, this review summarizes current “best practices” to be employed for chemical shift calculation to minimize computational sources of error. Functionals such as B3LYP and mPWP191 in combination with triple-zeta valence polarized basis sets such as 6-311+G(2d,p) yield good agreement with experiment for the purposes of structural assignment. Furthermore, instead of using a reference molecule such as tetramethylsilane, TMS, to convert shielding tensors into chemical shifts, computed values may be scaled linearly against the experimental data in hand or by using previously determined scaling constants for a test set of molecules. The Chemical Shift Repository (Cheshire) website<sup>32</sup> provides many of these scaling parameters, along with associated errors against a test set for  $^{13}\text{C}$  and  $^1\text{H}$  shifts. Sarotti and Pellegrinet have recently proposed an alternative to linear scaling, in which shielding tensors calculated for methanol and benzene at the same level are used as internal standards for hydrogens attached to  $\text{sp}^3$  and  $\text{sp}^2/\text{sp}$  hybridized carbons, instead of using a single standard such as TMS.<sup>33</sup> This so-called multi-standard (MTSD) method delivers lower average errors in relation to calculations using a TMS standard, and the basis set has only a small effect on the overall accuracy.

The structure of natural product aquatolide was confirmed experimentally following predictions made on the basis of DFT calculations of  $^{13}\text{C}$  and  $^1\text{H}$  chemical shifts, and  $^1\text{H}$ - $^1\text{H}$  coupling constants.<sup>34</sup> The originally proposed structure, containing an unusual ladderane substructure was considered computationally and found to result in large discrepancies, of up to 24 ppm for  $^{13}\text{C}$  and 1.3 ppm for  $^1\text{H}$ , between computed and the experimental chemical shifts. Based on biosynthetic considerations, and by analogy to other natural products Tantillo and co-workers proposed a structure for the natural product based on the [2+2] cyclization of the natural product asteriscunolide C (Fig. 10). Computed chemical shifts for this structure were in much more satisfactory agreement with experiment, and computed coupling constants predicted an unusually large  $^4\text{J}$  coupling constant of 6.8 Hz, also in agreement with experiment. The proposal was subsequently confirmed by X-ray crystallography. Stereochemistry was also elucidated for a 3-hydroxylated weltitindoline using a comparison of empirically scaled mPW1PW91/6-311+G(2d,p)  $^{13}\text{C}$  and  $^1\text{H}$  chemical shifts against experiment.<sup>35</sup> Mean absolute deviations (MADs) of 2.1 and 2.7 ppm were obtained for the two possible epimers computed with respect to the  $^{13}\text{C}$  spectrum, which did not allow for an unequivocal assignment to be made. However, one epimer matched the experimental  $^1\text{H}$  data much more closely than the other: MADs of 0.08 and 0.36 ppm were obtained for the two epimers, whilst the largest outlier for

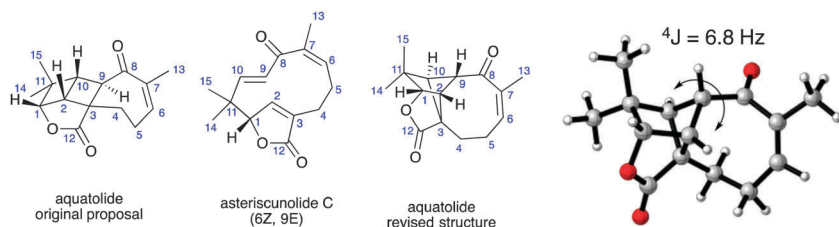


**Fig. 10** Original structure of aquatolide and reassigned structure on the basis of DFT computed  $^{13}\text{C}$  and  $^1\text{H}$  chemical shifts.

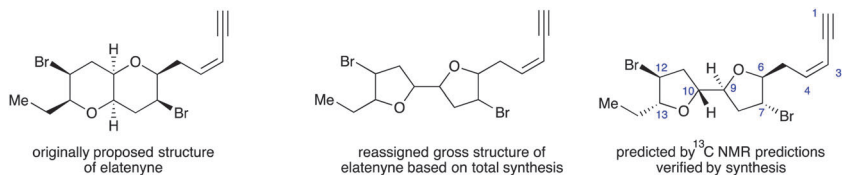


**Fig. 11** Original structure of elatenyne and reassigned structure on the basis of DFT computed  $^{13}\text{C}$  chemical shifts.

each was 0.13 and 0.79 ppm. This significant difference between the two diastereomers thus lent considerable confidence in the stereochemical assignment, which was later confirmed after alkylation of the alcohol showed interproton nOes to a remote vinyl group, confirming these groups as both on the same (concave) face of the molecule.

The use of DFT-based chemical shift calculations to assign the structure and stereochemistry of natural products has grown in use in recent years, particularly since the high profile reassignment of the structure of hexacyclinol by Rychnovsky in 2006.<sup>36</sup> Generally, although not always, these molecules have been rigid or cyclic structures since the number of conformations that may contribute to the ensemble-averaged chemical shifts is kept to a minimum. Bifulco, however, showed that NMR chemical shifts of flexible structures may be successfully computed, using the same theoretical methods provided an adequate conformational search is performed and the shifts are then averaged according to the conformer Boltzmann populations.<sup>37</sup> In 2012, two synthetic groups (Burton, Oxford and Kim, Seoul) independently verified the predicted structure of the natural product elatenyne (Fig. 11),<sup>38</sup> which has flexible side-chains, five-membered rings and a rotatable inter-ring torsion, but had nevertheless been predicted on the basis of GIAO chemical shift calculations in 2008 by Goodman and Burton.<sup>39</sup> For challenging cases of structural assignment, such as flexible molecules, those with remote stereocentres, or with groups with an uncertain protonation state, the use of chemical shift calculations may not allow a firm prediction to be made, or worse, favour the incorrect structure. Goodman has developed the DP4 metric<sup>40</sup> to gauge the significance of a given set of computed chemical shift errors in relation to a large test set and thus the level of confidence in a given structural assignment.

When different candidate structures have relatively similar chemical shifts their difference may be smaller than the inherent accuracy of the chemical shift calculations: in such cases it is advisable to use measurable data that exhibits greater variation between the structures so that computation may then discern between the possibilities. Butts and Bifulco have reported on the use of quantitative measurements of the nuclear Overhauser effect (nOe) to infer experimental interproton distances which may then be compared against values obtained from a calculation.<sup>41</sup> Since the intensity of the nOe between two protons varies as  $r^{-6}$  this is clearly a sensitive probe of stereochemistry and conformation that should be able to discern between relatively similar structures *e.g.* diastereoisomers. An internal standard is thus chosen for which the distance is known with high confidence, and relative intensities can thus be converted to absolute distances. The authors studied the polyhydroxylated steroid conicasterol F (Fig. 12), for which

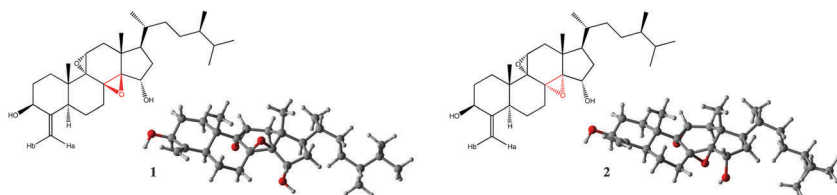


**Fig. 12** Diastereomers of conicasterol F differentiated by quantitative nOes.

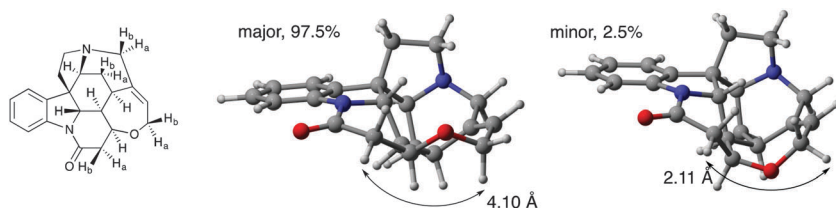


**Fig. 13** Two computed conformers of strychnine are necessary to explain the experimentally observed nOes.

the lack of protons at either end hampers the experimental assignment of the epoxide relative stereochemistry. A full conformational search using molecular dynamics and Monte Carlo simulations with MMFF were undertaken to generate low energy structures that were then optimized with DFT at the mPW1PW91/6-31G(d) level. The comparison of DFT optimized and experimental interproton distances show a clear difference: the mean absolute error and standard deviation for structure 1 is 3.0% and 2.6%, while for its diastereoisomer 2 these values are 7.8% and 5.9%.

Butts and Harvey have shown that nOe-based quantitative measurement of the  $H_{11b}$ – $H_{23b}$  distance in strychnine gave a distance of 3.49 Å, far shorter than expected from DFT or crystallographic structures (Fig. 13).<sup>42</sup> An additional low energy conformer level was subsequently located at the B3LYP/6-31G(d) level of theory with a much shorter H–H distance which contributes to the ensemble average value. The B3LYP relative energy of this conformer at 12.9 kJ mol<sup>−1</sup> is, however, rather higher than expected and gives too small a population to affect the equilibrium average. Calculations with more demanding correlated *ab initio* methods, such as LCCSD(T0), give a reduced solution energy difference of 9.4 kJ mol<sup>−1</sup> corresponding to a 2.2% population of this minor conformer, and an ensemble average of 3.6 Å which compares well with the experimental distance.

## 5 Reaction dynamics

### 5.1 Trajectory studies of organic reactions

Computational studies of reaction mechanisms often employ transition state theory (TST) with great success, explaining kinetically controlled product distribution in terms of the relative free energy barrier heights calculated for competing transition states. However, recent developments in theory and computing power have meant that realistic reaction mechanisms can also be probed by computing

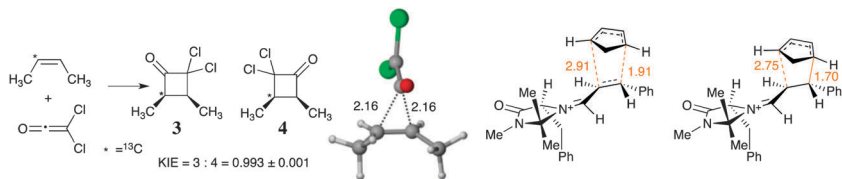


**Fig. 14** Isotopic effects in a [2+2] cycloaddition occurs due to differences in surface recrossing near the  $C_s$  symmetrical TS (shown centre). Variational TSs on the reaction path for an organocatalytic Diels–Alder reaction separated by an entropic intermediate.

dynamical trajectories along the reaction pathway point by point (“on the fly”) without the need for an analytical potential energy surface (PES). The number of examples continues to grow for which the statistical mechanics assumptions underlying classical TST are inadequate to explain experimentally observed selectivities; for example, redistribution of intramolecular vibrational energy may not be significantly faster than passage towards product(s), or trajectories may recross the barrier separating reactant and product states. In such cases the dynamical paths followed over the PES become critical. Singleton has reported the effects of isotopic labeling on the outcome of the [2+2] cycloaddition of dichloroketene with labeled *cis*-2-butene (Fig. 14).<sup>43</sup> The potential energy surface (computed at MPW1K, M06, and MP2 levels since B3LYP incorrectly predicts an unsymmetrical TS) shows an initial TS to form the first C–C bond with  $C_s$  symmetry, which then leads directly to a second symmetry breaking TS that bifurcates to the two isotopomeric cycloadducts. Applying conventional TST predicts that the two products will be formed in equal amounts, however, experimentally, the ratio of 3:4 is  $0.993 \pm 0.001$  (Fig. 14). Computing dynamical trajectories from the first TS the authors employ the trick of using an extremely heavy carbon atom (thus reducing the number of trajectories required to converge to a significant result). Product ratios for  $^{140}\text{C}$ ,  $^{76}\text{C}$ ,  $^{44}\text{C}$  and  $^{28}\text{C}$  are used to extrapolate to the predicted  $^{13}\text{C}$  result of 0.990, in excellent agreement with the experimental value. The origin of this isotopic effect is in surface recrossing: increased mass is found to result in less recrossing and thus lead more often to product. A statistical model using Rice–Ramsperger–Kassel–Marcus (RRKM) theory is also applied to explain the results, in which there is an entropic intermediate in-between the formation of the two C–C bonds, which also yields a predicted ratio of 0.992. Such a model is then applied to interpret the enantioselectivity of an imidazolidinone catalyzed Diels–Alder cycloaddition. Since bond formation is asynchronous again it may be argued that there is an entropic intermediate between formation of the two new C–C bonds, and it is a second variational TS on the free energy surface (as shown on the right in Fig. 14) that controls selectivity.

Singleton has also examined the role of dynamics in the nucleophilic substitution of a dichlorovinylketone (Fig. 15).<sup>44</sup> The experimental mixture of diastereoisomeric products is 81:19, however, analysis of all possible TSs at the B3LYP/6-31+G(d,p) level and by following the intrinsic reaction coordinate (IRC), computations predict that only one stereoisomer will be formed. Clearly this contradicts experiment and so quasiclassical dynamics calculations were performed, which showed that some trajectories from previously located TSs actually lead to the minor diastereoisomer

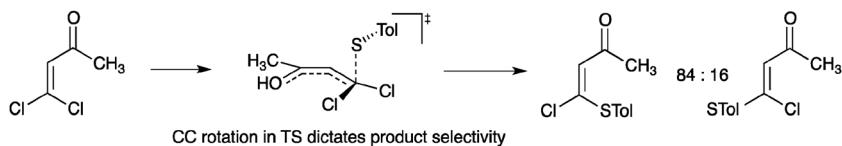


Fig. 15 Dynamically controlled nucleophilic substitution.

(*i.e.* they do not stick to the IRC) and result in a predicted ratio of 84:16. The conclusion is therefore that a dynamic effect controls selectivity, and that this effect is localized to a torsional rotation about the breaking C=C bond in the TS; it is only when this rotation is in a particular sense in the trajectories that the minor diastereomer may be formed.

Houk and Doubleday have used quasiclassical dynamics calculations to study the venerable Diels–Alder reaction to quantify the time between formation of the two new  $\sigma$ -bonds *i.e.* synchronicity.<sup>45</sup> An optimized TS geometry is given a set of atomic displacements and velocities taken from a Boltzmann distribution of the vibrational energy levels and the simulation is then run in both directions to produce each trajectory, and the initial conditions are sampled hundreds of times. The average time gap between formation of the two bonds (defined as when the C–C distance falls below 1.6 Å) is shown in Fig. 16 for the eight reactions studied. The TSs for reactions 1–5 and 7 are symmetrical and the dynamics trajectories show that the average time gaps between bond formation all fall below 5 femtoseconds (fs). The period for a C–C vibration is *ca.* 30–60 fs and so these six reactions may be reasonably classified as concerted and synchronous. Reactions 6 and 8 give rise to a small proportion, 2%, of trajectories where a diradical intermediate is formed on the timescale of 1000 fs, particularly at higher temperatures. However, while these reactions are more asynchronous, with time gaps of 15 and 57 fs they are still essentially concerted.

Tantillo and Hase have used direct dynamics simulations to study the conversion of the C<sub>20</sub> pimaradienyl cation to the abietadienyl cation, a key reaction step in the biosynthesis of abietadiene (Fig. 17).<sup>46</sup> This was previously shown to be the first biosynthetically relevant process to involve a potential energy surface with a bifurcating reaction pathway.<sup>47</sup> Trajectories initiated at the rate-controlling transition state (TS) that separates the pimaradienyl and abietadienyl cations

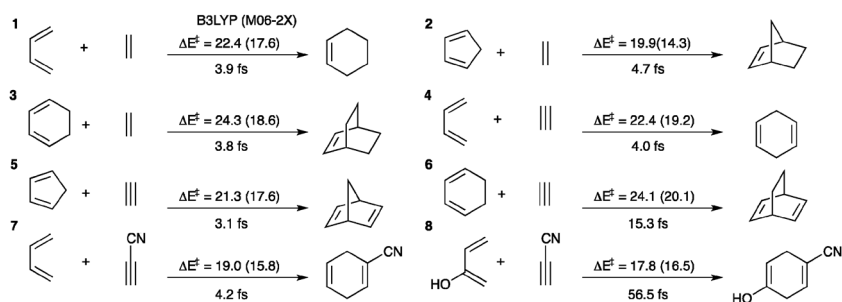
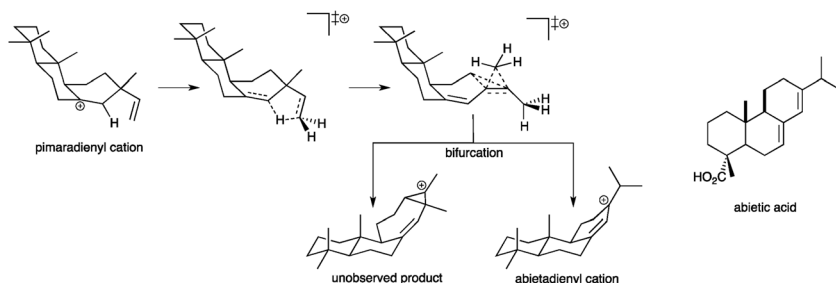


Fig. 16 Diels–Alder reactions activation barriers (kcal mol<sup>-1</sup>) and average time gaps (femtoseconds) between bond forming events.

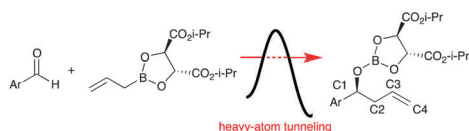


**Fig. 17** A reaction pathway bifurcation separates observed and unobserved products in enzymatic biosynthesis of abietic acid.

show that the  $C_{20}$  abietadienyl cation is generated in near equal amounts as a six and seven-membered ring. Since the seven-membered ring is not seen in nature, the simulation suggests that the abietadiene synthase enzyme is involved in dynamic steering of the reaction towards the natural product. Indeed the role of protein dynamics in enzyme catalysis is a matter of intense current debate.<sup>48</sup> Since experimental measurements of kinetic isotope effects for enzyme-catalyzed reaction have been found to show a complex dependence on temperature (particularly in the tunneling regime), it has been suggested that standard statistical rate theories, such as TST, are inadequate for their explanation. Glowacki and Mulholland instead argue that these data may still be interpreted in terms of a statistical theory provided the conformational behaviour of the enzyme is taken into account.<sup>49</sup> A model is presented in which two different enzyme:substrate conformations are in rapid equilibrium with each other, and in which the conformers lead to product formation with different rate constants. The TST may then be applied, including corrections for tunneling on the reaction rates to account for experimentally observed enzyme kinetics where protein dynamics has previously been invoked. The authors invoke Ockham's razor to argue that conformational sampling (in this case just two) is perhaps a more efficient way to explain the complex temperature-dependence in enzyme-catalyzed reactions. Since this model is based on TST it contradicts claims for a direct role for protein dynamics in 'driving' enzyme reactions.

## 5.2 Tunnelling effects

Recently Schreiner has demonstrated experimentally and through computation that the effects of quantum mechanical tunneling (QMT) can no longer be ignored in organic chemistry.<sup>50</sup> In a review on the topic of QMT in 2012,<sup>51</sup> Schreiner summarizes the state of the art, emphasizing the role of QMT on controlling not just absolute rate constants but also product selectivities. Indeed, the isomerizations of matrix isolated alkyl and aryl hydroxycarbenes are only permitted due to the effects of QMT since the activation barriers are too high for thermal activation. The role of heavy-atom tunneling in organic reactions is also emphasized, in the reactivity of the cyclopropylcarbinyl radical which displays relatively large effects of heavy-atom tunneling at  $-100\text{ }^{\circ}\text{C}$ . In the context of heavy atom tunneling, Singleton has investigated the allylboration reaction developed by Roush, where a diisopropyl tartrate ligand (DIPT) is used on boron to impart



	C1	C2	C3	C4
<i>Conventional TST KIEs</i>				
gas phase	1.038	1.026	0.997	1.018
PCM	1.041	1.025	0.998	1.016
<i>Corrected for tunneling and recrossing:</i>				
gas phase	1.047	1.036	0.998	1.020
PCM	1.052	1.038	0.999	1.019
<i>Experimental</i>				
	1.052	1.036	0.997	1.019

**Fig. 18**  $^{13}\text{C}$  Kinetic isotope effects in asymmetric allylboration show non-negligible contributions from tunneling and surface-recrossing.

stereoselectivity (Fig. 18).<sup>52</sup> The  $^{13}\text{C}$  kinetic isotope effects in this reaction are measured using Singleton's technique at natural abundance. Using the M06-2X/6-31+G(d,p) transition structure, however, the computed KIEs according to the method of Bigeleisen and Mayer are too small when compared with experiment. Thus the authors undertake to compute the corrections to these KIEs associated with the effects of multidimensional tunneling and surface recrossing on the reaction dynamics. It is found that the incorporation of these terms leads to much more satisfactory agreement with experiment, and it is noted that for example at  $\text{C}_2$  the heavy-atom tunneling accounts for 34% of the KIE which is larger than the effect of zero-point energy. Tunneling is computed to account for acceleration in the reaction rate by 1.36 relative to in its absence, and thus plays a role in even a relatively simple organic reaction.

## 6 Methodological developments

Advances in electronic structure theory are undoubtedly essential in improving the accuracy and applicability of computation to realistic chemical systems: nevertheless, our intention here is to emphasize recent developments in applied computational chemistry and in accurately modelling organic systems with a reasonable degree of computational cost. Tantillo and co-workers have described innovations implemented in an applied computational-theoretical chemistry laboratory, including tactile drawings, molecular model kits, and three-dimensional printing to provide access for blind or visually impaired students to explore structure-function relationships with minimal assistance from sighted co-workers.<sup>53</sup>

### 6.1 The role of dispersion

The failure of many commonly-used DFT functionals in common use to adequately describe medium and long range molecular interactions has become increasingly apparent as increases in computing power have enabled calculations to be performed on ever larger systems where these interactions may tend to accumulate. Further evidence was reported in 2012 that correcting for the missing dispersion energy of many of the widely-used density functionals (*e.g.* B3LYP) may be essential to capture even the more qualitative aspects involved in computational organic chemistry. Grimme reported benchmark studies on the geometries and strain energies of a series of cyclophanes, which, containing interannular distances of 3–3.2 Å constitute examples where medium-range correlation effects are important.<sup>54</sup> While B3LYP predicts equilibrium separations 0.1 Å too long

compared to the solid state, dispersion corrected functionals such as PW6B95-D3 and TPSS-D3 yield inter-ring distances essentially in accord with experiment. Grimme's D3 dispersion correction has seen much application in computational organic investigations since its publication in 2010.<sup>55</sup> In its original form this additive term is damped to zero at shorter interatomic distances, allowing the DFT exchange–correlation to “take over” in describing short range correlation. However, Becke and Johnson's modified (BJ) D3 damping function<sup>56</sup> instead dies away to a constant value at short distances to give much better calculated strain energies for the cyclophanes where an accurate description of medium-range correlation appears to be essential. Grimme has also reported protein–ligand binding energies computed with dispersion-corrected DFT, with the B97D-D3 functional applied to complexes containing up to 4000 atoms.<sup>57</sup> The molecular fractionation with conjugate caps (MFCC) approach approximates the protein–ligand binding energy as the summation of interactions between the ligand and individually capped protein fragments, and was used to estimate the *ab initio* binding energy of mitochondrial matrix adenylate kinase with its substrate AMP. Harvey and Mulholland have also explored the effects of including a dispersion correction in biochemical applications, by focussing on the optimized transition structures and activation barriers in QM/MM calculations for reactions of P450 enzymes with organic substrates.<sup>58</sup> Optimizations on the (D2) dispersion-corrected potential energy surface cause subtle changes on the TS geometries in relation to the uncorrected results, however, lower activation barriers result (*ca.* 5 kcal mol<sup>-1</sup>).

At low temperatures small linear alkanes prefer to adopt an extended all-*trans* conformation, however, as the chain length is increased there is a transition from this global energy minimum to a folded hairpin structure, which maximizes self-solvation due to dispersion interactions (Fig. 19). The interesting question of what is the longest alkane to adopt an extended chain conformation has been the subject of semi-empirical and molecular mechanics studies in the past, however, Mata and Suhm reported high level *ab initio* calculations and Raman spectroscopy performed on supersonic jet expansions at 10 K.<sup>59</sup> Local MP2 with density fitting (DF-LMP2) was used for optimizations, and the conformational energies were corrected with explicitly correlated coupled cluster CCSD(T0) energetics: this was restricted to local orbital pairs within 8 bohr, while nearby orbital pairs used a larger basis set. The computations show that C<sub>16</sub>H<sub>34</sub> and

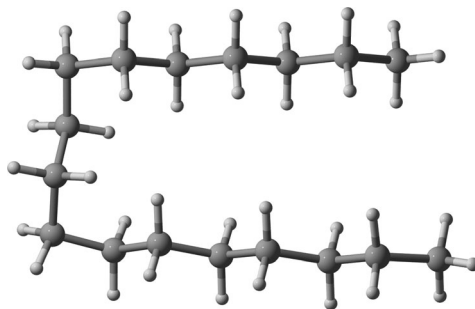
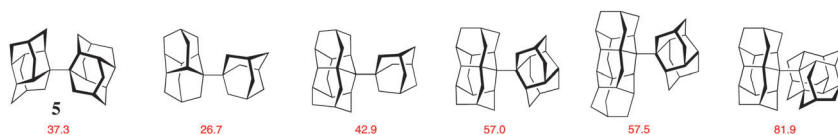


Fig. 19 Hairpin conformation of C<sub>17</sub>H<sub>36</sub>.



**Fig. 20** Diamondoids synthesized and examined computationally in ref. 60, with B3PW91/6-31G(d,p) strain energies in kcal mol<sup>-1</sup> relative to unstrained hydrocarbons.

smaller alkanes adopt a straight chain conformation, but that longer alkanes preferentially adopt the hairpin form. Experimental low-frequency Raman jet spectra were recorded for hexadecane (C<sub>16</sub>) to eicosane (C<sub>20</sub>) and fit to simulated spectra to estimate the hairpin: all-*trans* conformational ratios. These results suggest that C<sub>18</sub>H<sub>38</sub> is the last linear alkane to show appreciable amounts of the straight-chain conformation, however, due to the non-equilibrium nature of the low temperature experiments and quantum-statistical reasoning it is argued that C<sub>17</sub>H<sub>36</sub> is more likely to be the current best estimate.

Schreiner has synthesized sterically congested molecules, diamondoids, with extremely long C–C bonds over 1.7 Å shown in Fig. 20.<sup>60</sup> These molecules pose a significant challenge for DFT calculations since there are numerous dispersion interactions which effect bonding strength and rotational barriers. Previously Schreiner has shown that dispersion interactions may even be necessary to hold extremely strained molecules together, preventing heterolytic cleavage. Thus diamondoids provide a very rich testing ground for the range of currently available density functionals. For molecule 5, the crystallographically determined central C–C distance is 1.647 Å. Testing a variety of popular functionals with double-zeta basis sets (6-31G(d) or cc-pVDZ) leads to the conclusion that the functionals BLYP, B3LYP, B98, B97D, and B3PW91 all lead to optimized geometries where this bond is too long, presumably resulting from medium or long range correlation errors. Explicitly dispersion corrected functionals such as B3LYP-D and ωB97XD lead to acceptable distances, as does M06-2X and scs-MP2 and B2LYP-D methods. Clearly dispersion is important not only in evaluating energetics but also in geometry optimization. The rotational barrier for this central bond is estimated from variable temperature NMR to be 16 kcal mol<sup>-1</sup> which again is used to benchmark various functionals. Interestingly here, the functionals which provide the best geometric description fare much worse in their prediction of the rotational barrier, with M06-2X, ωB97X-D and B3LYP-D yielding values which are too large by 2.5 to 3.5 kcal mol<sup>-1</sup>. Functionals performing well for this barrier height, conversely, are rather poor at describing the bond distance, such B3LYP, B97D and PBE1PBE and B3PW91. Presumably this is a fortuitous result of overestimating the C–C bond length, however, this emphasizes the challenge of accurately describing medium-range correlation using DFT.

The use of DFT calculations in estimating the binding free energies of relatively large supramolecular clusters (300–400 atoms) in solution was reported.<sup>61</sup> Employing D3 dispersion corrected DFT methods gives impressive typical errors of only 1–2 kcal mol<sup>-1</sup> in relation to experiment, further demonstrating the usefulness of such corrections in the study of larger, “real-life” chemical systems. Important recommendations are the inclusion of three-body dispersion effects,

which have previously proved to be unimportant in small benchmark systems; these have to be included to avoid computational overbinding, whilst the entropy due to the low-frequency vibrational modes must also be described using the simple free-rotor approximation rather than the standard harmonic approximation,<sup>62</sup> which can cause unpredictable errors for entropy differences and often introduce significant noise into the total free enthalpy results.

## 6.2 Basis set considerations

Computations of complexation, or bimolecular reactions are known to suffer from basis set superposition error (BSSE), due to the fact that basis functions centered on one of the monomers are used to supplement the basis set of the other. This then represents a better description of each monomer, and so introduces an inconsistency in the way the monomers are described as a function of their separation. BSSE always increases the calculated binding energy in the complex or TS and leads to artificial shortening of intermolecular distances. One potential and widely-used correction for this unphysical effect was proposed by Boys and Bernardi in 1970,<sup>63</sup> which corrects for the superposition by computing the energy of each monomer in the presence of the basis functions, but none of the nuclei or electrons of the partner. However, this can be costly to perform and so a more efficient semi-empirical approach has been proposed in 2012 by Grimme.<sup>64</sup> An additive geometric counterpoise correction (gCP) is defined which depends on the interatomic distances, the interatomic overlap integrals for a single Slater orbital taken from extended Hückel theory, and the number and availability of virtual (*i.e.* unoccupied) orbitals centred on each atom. Parameterization has been performed for specific combinations of density functional and basis sets, so for example the B3LYP/6-31G(d) method can be corrected to obtain results that are similar to the complete basis set limit. These corrections can be performed using a web server available from Grimme.<sup>65</sup> The applicability of this approach is shown in a study of benchmark sets for basic properties,

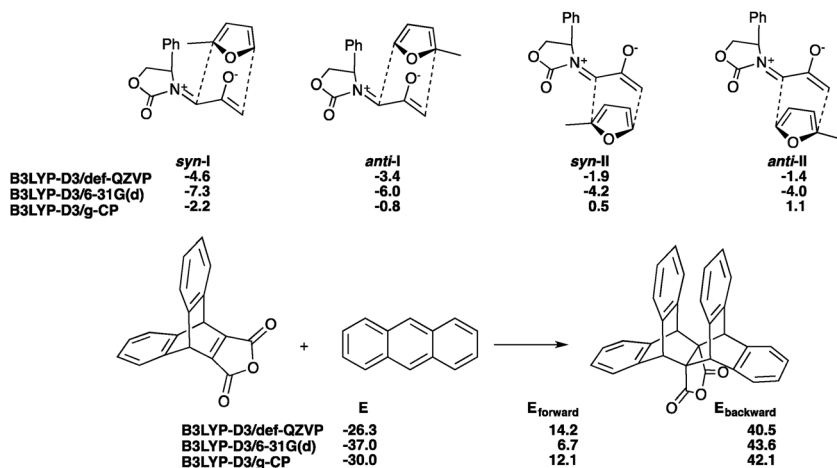


**Fig. 21** Geometric counterpoise correction applied to B3LYP/6-31G(d) energy changes in organic cycloadditions.

reaction energies and non-covalent interactions, where B3LYP/6-31G(d) results are corrected with a D3 dispersion term and the gCP counterpoise correction to yield results comparable to, and in many cases superior to calculations with a much more expensive def2-QZVP basis set.<sup>66</sup> Examples of organic reactions are considered, such as the [4+3] cycloaddition of an oxallyl with furan and an anthracene and maleimide cycloaddition, where incorporation of the gCP counterpoise term results in complexation energies and activation barriers in much closer agreement with def-QZVP results than for uncorrected values which are substantially too negative (Fig. 21).

## 7 Computational organic chemistry on the web

It seems right for a review of computational organic chemistry in 2013 to recognise the growing influence of web-based material, such as blogs, and digital-only journals on the field. Prof. Steven Bachrach's blog *Computational Organic Chemistry*<sup>67</sup> regularly highlights papers in the field and includes interactive structures that may be rotated in a web-browser. Prof. Henry Rzepa's blog<sup>68</sup> is also recommended reading for those interested in both computational and organic chemistry: ideas are thoughtfully explored through calculations, for example whether cyclobutadiene and carbon dioxide can co-exist in a calixarene host, or the thermodynamics of the Finkelstein nucleophilic substitution. Rzepa's blog also highlights how computation and 3D molecular visualization of structures may be used to lend pedagogic insight into many archetypal phenomena from organic chemistry in a clear and refreshing way. The results of these calculations are also archived in an institutional repository so that readers may access and re-use original data in a much easier way than from, for example, supplementary PDFs that accompany many journals. Finally, the overlay journal *Computational Chemistry Highlights*<sup>69</sup> is a web only aggregation of recent articles spanning all sorts of computational chemistry research, including computational organic, where papers are selected and summarized by an editorial board of practitioners in the field.

## References

- 1 S. M. Bachrach, *Annu. Rep. Prog. Chem., Sect. B: Org. Chem.*, 2008, **104**, 394.
- 2 S. M. Bachrach, *Annu. Rep. Prog. Chem., Sect. B: Org. Chem.*, 2009, **105**, 398.
- 3 S. M. Bachrach, *Annu. Rep. Prog. Chem., Sect. B: Org. Chem.*, 2010, **106**, 407.
- 4 S. M. Bachrach, *Annu. Rep. Prog. Chem., Sect. B: Org. Chem.*, 2011, **107**, 349.
- 5 S. M. Bachrach, *Annu. Rep. Prog. Chem., Sect. B: Org. Chem.*, 2012, **108**, 334.
- 6 J. F. Gonthier, S. N. Steinmann, M. D. Wodrich and C. Corminboeuf, *Chem. Soc. Rev.*, 2012, **41**, 4671.
- 7 Y. Mo, *Nat. Chem.*, 2010, **2**, 666.
- 8 Y. Mo, P. Bao and J. Gao, *Phys. Chem. Chem. Phys.*, 2011, **13**, 6760.
- 9 C. Wang, F. Ying, W. Wu and Y. Mo, *J. Am. Chem. Soc.*, 2011, **133**, 13731.
- 10 Y. Mo and J. Gao, *Acc. Chem. Res.*, 2007, **40**, 113.
- 11 J. I. Wu, I. Fernández, Y. Mo and P. v. R. Schleyer, *J. Chem. Theory Comput.*, 2012, **8**, 1280.
- 12 S. E. Wheeler, K. N. Houk, P. v. R. Schleyer and W. D. Allen, *J. Am. Chem. Soc.*, 2009, **131**, 2547.
- 13 X. Bao, D. A. Hrovat and W. T. Borden, *J. Org. Chem.*, 2012, **77**, 956.
- 14 J. I.-C. Wu, Y. Mo, F. A. Evangelista and P. v. R. Schleyer, *Chem. Commun.*, 2012, **48**, 8437.
- 15 W. C. McKee, J. I. Wu, M. Hofmann, A. Berndt and P. V. R. Schleyer, *Org. Lett.*, 2012, **14**, 5712.

- 16 B. Gold, N. E. Shevchenko, N. Bonus, G. B. Dudley and I. V. Alabugin, *J. Org. Chem.*, 2012, **77**, 75.
- 17 (a) P. H. Y. Cheong, R. S. Paton, S. M. Bronner, G. Y. Im, N. K. Garg and K. N. Houk, *J. Am. Chem. Soc.*, 2010, **132**, 1267; (b) A. E. Goetz, S. M. Bronner, J. D. Cisneros, J. M. Melamed, R. S. Paton, K. N. Houk and N. K. Garg, *Angew. Chem., Int. Ed.*, 2012, **51**, 2758.
- 18 K. Gilmore, M. Manoharan, J. I.-C. Wu, P. V. R. Schleyer and I. V. Alabugin, *J. Am. Chem. Soc.*, 2012, **134**, 10584.
- 19 P. v. R. Schleyer, C. Maerker, A. Dransfeld, H. Jiao and N. J. R. van Eikema Hommes, *J. Am. Chem. Soc.*, 1996, **118**, 6317.
- 20 S. Shaik, D. Danovich, W. Wu, P. Su, H. S. Rzepa and P. C. Hiberty, *Nat. Chem.*, 2012, **4**, 195.
- 21 A. Grushow, *J. Chem. Educ.*, 2011, **88**, 860.
- 22 C. Landis and F. Weinhold, *J. Chem. Educ.*, 2012, **89**, 570.
- 23 P. C. Hiberty, F. Volatron and S. Shaik, *J. Chem. Educ.*, 2012, **89**, 575.
- 24 L. Simón and J. M. Goodman, *J. Org. Chem.*, 2011, **76**, 1775.
- 25 M. N. Grayson, S. C. Pellegrinet and J. M. Goodman, *J. Am. Chem. Soc.*, 2012, **134**, 2716.
- 26 L. Simón and J. M. Goodman, *J. Am. Chem. Soc.*, 2012, **134**, 16869.
- 27 See: P. H.-Y. Cheong, C. Y. Legault, J. M. Um, N. Çelebi-Ölçüm and K. N. Houk, *Chem. Rev.*, 2011, **111**, 5042 and references therein.
- 28 S. Mitsumori, H. Zhang, P. H.-Y. Cheong, K. N. Houk, F. Tanaka and C. F. Barbas, *J. Am. Chem. Soc.*, 2006, **128**, 1040.
- 29 Y. Lam, K. N. Houk, U. Scheffler and R. Mahrwald, *J. Am. Chem. Soc.*, 2012, **134**, 6286.
- 30 G. Sahoo, H. Rahaman, A. Madarász, I. Pápai, M. Melarto, A. Valkonen and P. M. Pihko, *Angew. Chem., Int. Ed.*, 2012, **51**, 13144.
- 31 M. W. Lodewyk, M. R. Siebert and D. J. Tantillo, *Chem. Rev.*, 2012, **112**, 1839.
- 32 M. W. Lodewyk, M. R. Siebert and D. J. Tantillo, <http://cheshirenmr.info>.
- 33 A. M. Sarotti and S. C. Pellegrinet, *J. Org. Chem.*, 2012, **77**, 6059.
- 34 M. W. Lodewyk, C. Soldi, P. B. Jones, M. M. Olmstead, J. Rita, J. T. Shaw and D. J. Tantillo, *J. Am. Chem. Soc.*, 2012, **134**, 18550.
- 35 K. W. Quasdorf, A. D. Hutters, M. W. Lodewyk, D. J. Tantillo and N. K. Garg, *J. Am. Chem. Soc.*, 2012, **134**, 1396.
- 36 S. D. Rychnovsky, *Org. Lett.*, 2006, **8**, 2895.
- 37 G. Barone, D. Duca, A. Silvestri, L. Gomez-Paloma, R. Riccio and G. Bifulco, *Chem.-Eur. J.*, 2002, **8**, 3240.
- 38 B. S. Dyson, J. W. Burton, T.-I. Sohn, B. Kim, H. Bae and D. J. Kim, *J. Am. Chem. Soc.*, 2012, **134**, 11781.
- 39 S. G. Smith, R. S. Paton, J. W. Burton and J. M. Goodman, *J. Org. Chem.*, 2008, **73**, 4053.
- 40 S. G. Smith and J. M. Goodman, *J. Am. Chem. Soc.*, 2010, **132**, 12946.
- 41 M. G. Chini, C. R. Jones, A. Zampella, M. V. D'Auria, B. Renga, S. Fiorucci, C. P. Butts and G. Bifulco, *J. Org. Chem.*, 2012, **77**, 1489.
- 42 C. P. Butts, C. R. Jones and J. N. Harvey, *Chem. Commun.*, 2011, **47**, 1193.
- 43 O. M. Gonzalez-James, E. E. Kwan and D. A. Singleton, *J. Am. Chem. Soc.*, 2012, **134**, 1914.
- 44 X. S. Bogle and D. A. Singleton, *Org. Lett.*, 2012, **6**, 2528.
- 45 K. Black, P. Liu, L. Xu, C. Doubleday and K. N. Houk, *Proc. Natl. Acad. Sci. U. S. A.*, 2012, **109**, 12860.
- 46 M. R. Siebert, P. Manikandan, R. Sun, D. J. Tantillo and W. L. Hase, *J. Chem. Theory Comput.*, 2012, **8**, 1212.
- 47 M. R. Siebert, J. Zhang, S. V. Addepalli, D. J. Tantillo and W. L. Hase, *J. Am. Chem. Soc.*, 2011, **133**, 8335.
- 48 S. Hay and N. S. Scrutton, *Nat. Chem.*, 2012, **4**, 161.
- 49 D. R. Glowacki, J. N. Harvey and A. J. Mulholland, *Nat. Chem.*, 2012, **4**, 169.
- 50 P. R. Schreiner, H. P. Reisenauer, D. Ley, D. Gerbig, C.-H. Wu and W. D. Allen, *Science*, 2011, **332**, 1300.
- 51 D. Ley, D. Gerbig and P. R. Schreiner, *Org. Biomol. Chem.*, 2012, **10**, 3781.
- 52 M. J. Veticatt and D. A. Singleton, *Org. Lett.*, 2012, **14**, 2370.
- 53 H. B. Wedler, S. R. Cohen, R. L. Davis, J. G. Harrison, M. R. Siebert, D. Willenbring, C. S. Hamann, J. T. Shaw and D. J. Tantillo, *J. Chem. Educ.*, 2012, **89**, 1400.
- 54 S. Grimme and C. Mück-Lichtenfeld, *Isr. J. Chem.*, 2012, **52**, 180.
- 55 S. Grimme, J. Antony, S. Ehrlich and H. Krieg, *J. Chem. Phys.*, 2010, **132**, 154104.
- 56 A. D. Becke and E. R. Johnson, *J. Chem. Phys.*, 2005, **122**, 154101.
- 57 J. Antony and S. Grimme, *J. Comput. Chem.*, 2012, **33**, 1730.
- 58 R. Lonsdale, J. N. Harvey and A. J. Mulholland, *J. Chem. Theory Comput.*, 2012, **8**, 4637.
- 59 N. O. B. Lüttschwager, T. N. Wassermann, R. A. Mata and M. A. Suhm, *Angew. Chem., Int. Ed.*, 2012, **1**, 463.

## Review

- 60 A. A. Fokin, L. V. Chernish, P. A. Gunchenko, E. Y. Tikhonchuk, H. Hausmann, M. Serafin, J. E. P. Dahl, R. M. K. Carlson and P. R. Schreiner, *J. Am. Chem. Soc.*, 2012, **134**, 13641.
- 61 S. Grimme, *Chem.–Eur. J.*, 2012, **18**, 9955.
- 62 R. F. Ribeiro, A. V. Marenich, C. J. Cramer and D. G. Truhlar, *J. Phys. Chem. B*, 2011, **115**, 14556.
- 63 S. F. Boys and F. Bernardi, *Mol. Phys.*, 1970, **19**, 553.
- 64 H. Kruse, L. Goerigk and S. Grimme, *J. Org. Chem.*, 2012, **77**, 10824.
- 65 S. Grimme, [www.thch.uni-bonn.de/tc/downloads/gcp/index.html](http://www.thch.uni-bonn.de/tc/downloads/gcp/index.html).
- 66 H. Kruse and S. Grimme, *J. Chem. Phys.*, 2012, **136**, 154101.
- 67 S. M. Bachrach, <http://comporgchem.com/blog/>.
- 68 H. S. Rzepa, <http://www.ch.imperial.ac.uk/rzepa/blog>.
- 69 <http://www.compchemhighlights.org>.